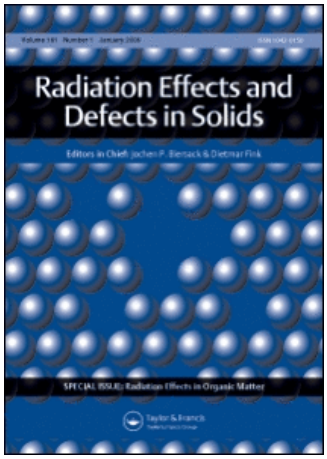

Radiation Effects and Defects in Solids
Publication details, including instructions for authors and subscription information:
http://www.informaworld.com/smpp/title~content=t713648881

Kinetics of the radiation-induced radical species in gamma irradiated solid sodium ascorbate

H. Tuner [a]; M. Korkmaz [a]
[a] Department of Physics Engineering, Faculty of Engineering, Hacettepe University, Beytepe, Ankara, Turkey

Online Publication Date: 01 February 2008
To cite this Article: Tuner, H. and Korkmaz, M. (2008) 'Kinetics of the radiation-induced radical species in gamma irradiated solid sodium ascorbate', Radiation Effects and Defects in Solids, 163:2, 95 - 105
To link to this article: DOI: 10.1080/10420150701284345
URL: http://dx.doi.org/10.1080/10420150701284345

Radiation Effects & Defects in Solids
Vol. 163, No. 2, February 2008, 95–105

Kinetics of the radiation-induced radical species in gamma irradiated solid sodium ascorbate

H. TUNER* and M. KORKMAZ

Department of Physics Engineering, Faculty of Engineering, Hacettepe University, 06800, Beytepe, Ankara, Turkey

(Received 22 January 2007; in final form 15 February 2007)

In the present work, radicals induced in γ-irradiated solid sodium ascorbate (SA) were studied by electron spin resonance (ESR) spectroscopy. While unirradiated samples presented no ESR signal, irradiated samples were found to present a spectrum of an unresolved doublet with a shoulder at the low-magnetic field side. Structural and kinetic features of the radical species responsible for the experimental ESR spectrum were explored through the variations of the signal intensities associated with spectrum maxima and minima with applied microwave power, sample temperature, and room temperature storage time. Activation energies of the involved species were also determined using the data derived from annealing studies performed at high temperatures. Produced radical species were observed to be relatively stable at room temperature. This gave the opportunity to distinguish irradiated SA or SA containing irradiation products from unirradiated ones even long after irradiation. SA presented also the features of a dosimetric material, which could be used in the estimation of dose range in accidental dosimetry.

Keywords: Electron spin resonance; Sodium ascorbate; Irradiation; Radical

1. Introduction

Vitamin C is one of the most important vitamins for humans who have to take it from fruits or drugs. The most important vitamin C source is ascorbic acid (AA). It is an acidic species and will contribute to gastric irritation in sensitive persons. Sodium ascorbate (SA) is used as the vitamin C source in pharmacy instead of AA. SA is, in fact, AA that has been neutralized with sodium until the taste is mild. AA and its sodium, potassium, and calcium salts are commonly used as a food additive in meat products, soft drink, jams, and quick frozen fish [1] due to their essential roles as an antioxidant and free radical scavenger.

Food irradiation is a cold process for preserving food and has been established as safe and effective method of food processing and preservation after more than five decades of research and development [2–10]. While irradiation creates positive effects by killing present microorganisms in irradiated foods or by inhibiting their activities in large extent, it also

*Corresponding author. Tel.: +90 312 297 72 13; Fax: +90 312 299 20 37; Email: htuner@hacettepe.edu.tr

Radiation Effects & Defects in Solids
ISSN 1042-0150 print/ISSN 1029-4953 online © 2008 Taylor & Francis
http://www.tandf.co.uk/journals
DOI: 10.1080/10420150701284345

causes damages in antioxidants added to foods for preservation purpose. In this respect, the knowledge of the radiation sensitivities of food additives is important. In the present work, kinetic features of the radicalic intermediates produced upon gamma irradiation of SA were studied as a part of an extensive project seeking to investigate the effects of gamma radiation on solid antioxidants using electron spin resonance (ESR) spectroscopy.

Effects of gamma radiation on solid SA have already been reported in a previous work [11], but room and high-temperature kinetic features, structures of the radical species produced after irradiation and their spectroscopic parameters were not reported up to present days. Yet, the knowledge about the stabilities of the radical species is important for the discrimination of SA containing irradiated foods from unirradiated ones, radiosterilization of SA, and dose estimation. Therefore, the aim of the present work is to determine room (290 K) and high-temperature (370, 380, 390, and 400 K) kinetic features, structures, and spectroscopic parameters of the radical species produced in gamma irradiated SA through annealing studies and spectrum simulation calculations, respectively.

2. Materials and methods

The SA samples of white to color crystalline solid with melting point 220 °C were provided from three drug companies [Eczacıbaşı, Istanbul; Merck (13, 873), Istanbul; and Aldrich (134-03-2), Ankara] and two food companies (Farmagen, Ankara and GMT Food Ingredients, Istanbul) and used without any further treatment by keeping them in sealed polyethylene vials at room temperature (290 K) in dark before irradiation. The molecular structure of SA is given in figure 1. It was prepared synthetically and, like AA (E300), SA (E301) is used as an antioxidant, color preservative and as a vitamin supplement in the food industry. Crystalline solid SA with 0.1 wt% water content was directly transferred to polycarbonate vials for irradiation treatment. All irradiation and ESR experiments were carried out on samples open to air in order to stay under commercial food irradiation and radiation sterilization conditions, and to explore the possible dosimetric use of SA as a normal and/or accidental dosemeter. All irradiations were performed at room temperature (290 K) using ^{60}Co-γ source supplying a dose rate of 1.8 kGy/h in the sample position at the Sarayköy Nuclear Research Center of Turkish Atomic Energy Agency in Ankara. The source was calibrated against a Fricke ferrous sulphate dosemeter, and the dose rate at the site of the irradiated samples was calculated by applying appropriate

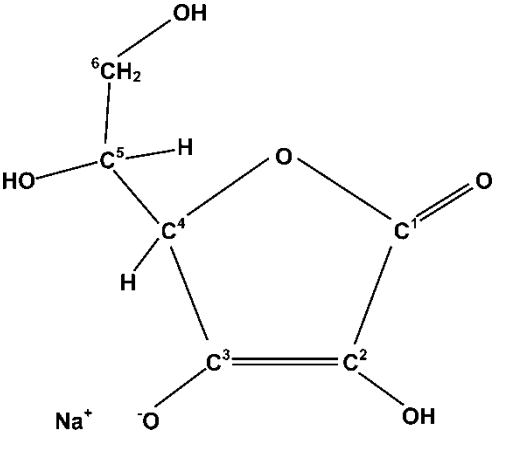

Figure 1. Molecular structure of SA.

corrections on the basis of the photon mass attenuation and energy-absorption coefficient for the sample and the dosemeter solution. Irradiated samples were kept at room temperature at dark in polycarbonate vials during the entire experiments. A set of 20 samples irradiated to doses 0.5, 1.0, 2.0, 5.0, 7.0, 10.0, 15.0, 20.0, and 25.0 kGy was employed to construct the dose–response curve. Samples prepared from SA irradiated to a dose of 15 kGy were used both to investigate structural and spectral features of the contributing radical species and to study the kinetic features of radiation-induced radical species at four different annealing temperatures (370, 380, 390, and 400 K).

After being irradiated in polycarbonate vials, ESR measurements were taken on the samples transferred into quartz ESR tubes of 4 mm inner diameter using a Bruker EMX-131 X-band ESR spectrometer operating at 9.7 GHz and equipped with a high-sensitive cylindrical cavity. The conditions of operation were: central field, 348 mT; scan range, 7 mT; microwave power, 0.4 mW; microwave frequency 9.782 GHz; receiver gain, 2.52×10^4; modulation frequency, 100 kHz; sweep time, 83.89 s. The sample temperature inside the microwave cavity was monitored with a digital temperature control unit (Bruker ER 411-VT). The latter provided the opportunity of measuring the temperature with an accuracy of ± 0.5 K at the site of the sample. A cooling, heating, and subsequent cooling cycle was adopted to monitor the free radical signal evolution. The temperature of the samples was first decreased to 120 K, starting from room temperature with an increment of 20 K, then increased to 400 K, and finally decreased again to room temperature.

Kinetic behaviors of the involved radical species were evaluated at four different temperatures. To attain this goal, the samples were heated to a predetermined temperature and kept at this temperature for a predetermined time, then, the spectra were recorded at annealing temperatures without cooling the samples to room temperature. The position of the sample in the cavity was not changed during the long-term signal intensity decay experiment at room temperature to avoid any error in signal intensity measurements arising from changes in the cavity-filling factor. All results are given as the replicate of three different measurements performed using three different samples.

3. Experimental results and discussion

3.1 *Room temperature results*

Although unirradiated SA exhibited no ESR signal, irradiated SA showed a simple ESR spectrum of unresolved doublet appearance spread over a magnetic field range of 1.5 mT and centered at $g = 2.0057$ as shown in figure 2a and b. That was the case for all studied SA samples provided from drug and food companies. The pattern of the spectrum with many maxima and minima was observed not to depend on the applied radiation dose, microwave power, and temperature in the ranges of the 0.5–25 kGy, 0.0016–10 mW, and 120–400 K, respectively. This spectrum is quite different from that reported in the literature [11] for the same compound. While the spectrum for SA given in ref. [11] has a singlet appearance, the spectrum given in figure 2 appears to be an unresolved doublet or a singlet with very different orthorhombic g tensor components. The ESR spectrum of gamma irradiated SA is also very different from the room temperature ESR spectrum of irradiated AA [11–13]. Two intense resonance lines with a separation of 2.7 mT dominate the AA ESR spectrum. However, the ESR spectrum of SA is spread over a magnetic field of 1.5 mT. In other words, the ESR spectrum of AA turns out to be deeply affected by its neutralization with sodium.

Studies carried out in the present work were based on the evolutions of the I_1, I_2, I_3, I_4, and I_5 signal intensities measured with respect to the spectrum base line (figure 2b). Microwave

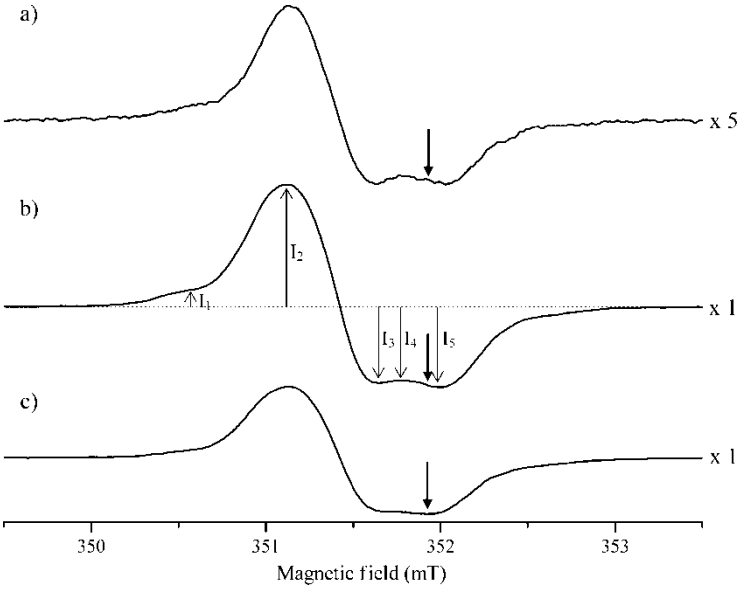

Figure 2. ESR spectra of SA samples irradiated at two different doses. (a) and (b) room temperature (290 K) [(a) 1 kGy, 0.4 mW; (b) 10 kGy, 0.4 mW]; (c) 10 kGy, 120 K, 0.004 mW. Bold arrows indicate the position of the diphenylpicrylhydrazyl (DPPH) g value ($g = 2.0036$).

saturation characteristics of the mentioned intensities were investigated first at room temperature (290 K) and at 120 K using a sample irradiated at a dose of 10 kGy. All intensities except for I_1 exhibited the characteristic behavior of homogeneously broadened resonance lines at both temperatures, that is, an increase at low powers, and then a decrease at high powers (figure 3a and b). Both increase and decrease rates and microwave saturation powers at 290 and 120 K were different for the observed intensities and, as is expected, they saturated at lower microwave power at 120 K. Differently from our results, an inhomogeneously broadened microwave saturation behavior has been reported for gamma irradiated SA in ref [11].

3.2 *Variable temperature studies*

Temperature is an important parameter in the determination of characteristic features of the involved radicals contributing to the formation of experimental ESR spectra. Namely, changes in the signal intensities with temperature can give novel information concerning the stabilities and number of radical types created upon irradiation. Preliminarily to the study, care was taken with the use of microwave power to avoid saturation even at the lowest temperature achievable in the present work (120 K). Thus, a microwave power of 0.0025 mW was adopted throughout the variable temperature studies. Variations of the denoted intensities (figure 2b) with temperature were investigated in the temperature range of 120–400 K using a sample irradiated to a dose of 10 kGy. Cooling the sample from room temperature (290 K) down to 120 K produced similar continuous increases in all intensities. Examples of these variations are illustrated in figure 4 for I_2 and I_5 intensities. When the sample was heated again from 120 K to room temperature, the intensity curves followed the same path in a reversible way and reached their initial values before cooling. Heating of the sample above room temperature produced irreversible continuous decreases in the investigated intensities (figure 4) without causing any pattern changes implying the radical decay at high temperatures. However, the decays in the signal intensities were not same for all observed resonance lines predicting the

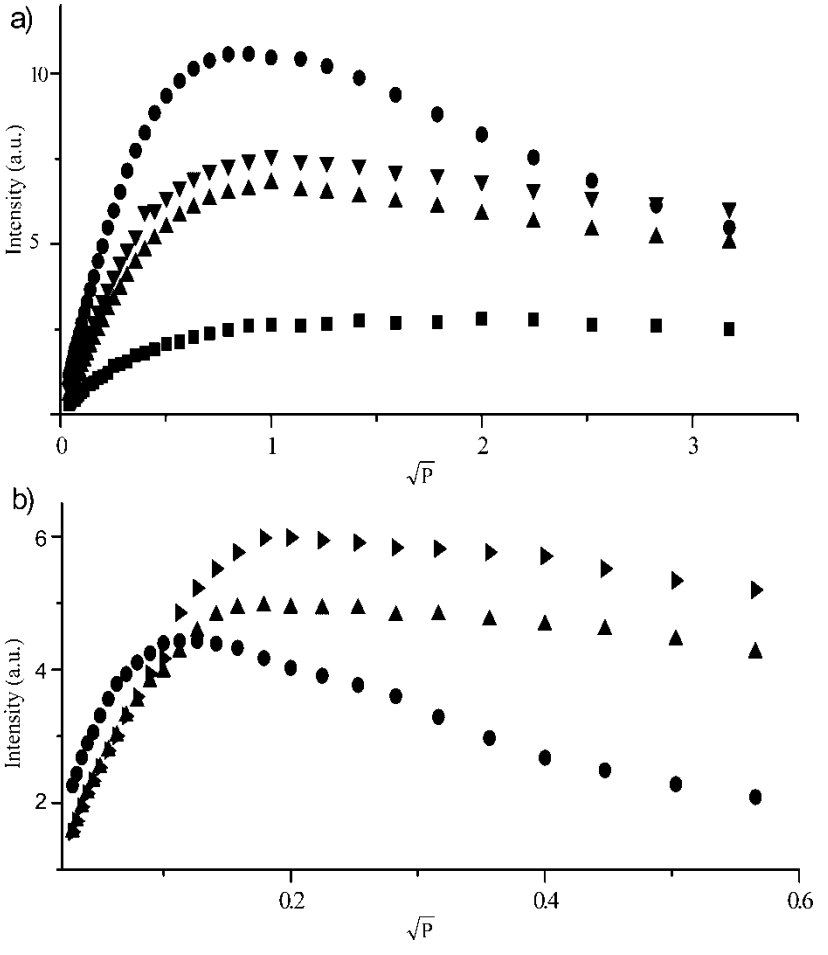

Figure 3. Microwave saturations at two different temperatures of the measured intensities for a sample irradiated at a dose of 10 kGy. (a) 290 K (■(I_1); ●(I_2); ▲(I_4); ▼(I_5)); (b) 120 K (●(I_2); ▶(I_3); ▲(I_4)).

presence of more then one radical specie in irradiated SA. Comparison of the signal intensities calculated from room temperature spectra of a sample before and after heating up to 400 K, and then cooling to room temperature indicated intensity decreases <5%. This was considered as verifying relatively high stabilities of the radicals produced in the irradiated SA.

3.3 *Room temperature signal intensity decreases in long term*

The long-term radical stability is one of the most important parameters in ESR dosimetry and in discrimination of irradiated samples from unirradiated ones. Furthermore, the intensity variation in the long term can help in the determination of radical types. To explore the aforementioned features of the radicals produced in gamma irradiated SA, a sample with 0.1 wt% water content irradiated at a dose of 10 kGy was stored at room temperature in dark and its spectra were recorded in regular time intervals over a storage period of 90 days. Then, the graphs of signal intensity versus storage time were constructed using the data derived from these spectra for the denoted resonance lines (figure 2b). Data relevant to I_2 and I_5 intensities are presented in figure 5. The long-term signal intensity data were observed to exhibit a

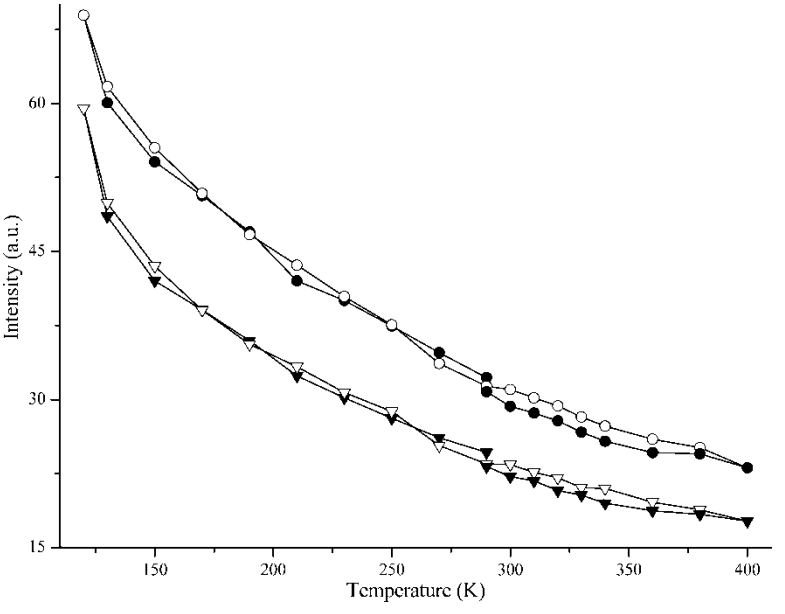

Figure 4. Variations of the I_2 and I_5 intensities with temperature for a sample irradiated at a dose of 10 kGy. Cooling 290 → 120 K and 400 → 290 K: •(I_2); ▲(I_5); heating 120 → 400 K: ∘(I_2); ▽(I_5).

biphasic decay character. While investigated intensities stayed almost constant during the first 40 days of storage, thereafter they began to undergo relatively low decreases. The calculated decreases were 7% and 5% for I_2 and I_5 intensities, respectively, at the end of the 90-day storage period. Other lines experienced lesser decreases. The loss of a small number of water molecules could be assigned to the origin of the observed weak intensity decreases.

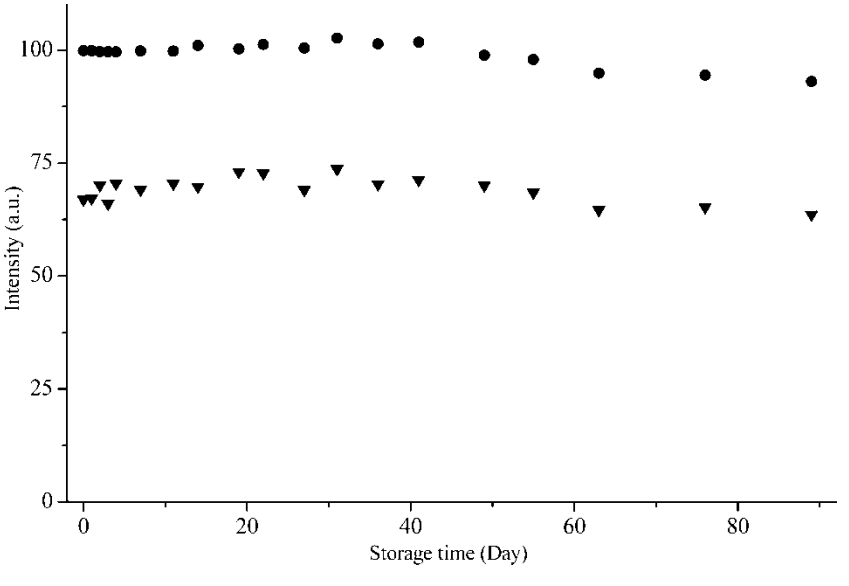

Figure 5. Variations of the I_2 and I_5 intensities with storage time at room temperature. •(I_2); ▼(I_5).

3.4 *Dose-response curves*

Besides the qualitative discrimination of irradiated samples from non-irradiated ones, ESR spectroscopy is also used for dose estimation [3–7] and dose measurement [7, 8]. However, the critical point for accurate dose estimation is the choice of the mathematical functions used to describe the dose–response curves. Linear, polynomial, and exponential functions are frequently used for this purpose [11, 12, 14–16]. Samples irradiated at doses 0.5, 1.0, 2.0, 5.0, 7.0, 10.0, 15.0, 20.0, and 25.0 kGy were used to construct dose–response graphs. Signal intensities calculated from recorded spectra were normalized to mass of samples and spectrometer gain and they were used to construct dose–response graphs, namely, the variations of the normalized signal intensities with applied radiation dose. The results are presented in figure 6. Mathematical functions given in table 1 were tried to fit the experimental dose–response data in the present work. It was concluded that a polynomial function of applied dose, that is, a function of the type $I = a + bD + cD^2$, where I and D stand for intensity and applied dose, respectively, and a, b, and c are the constants to be determined, describes best the experimental data. Calculated values of the constants and corresponding correlation coefficients from the studied intensities are given in table 1. As can be seen from this table, a polynomial function correlates reasonably well with the experimental data derived from the studied signal intensities in the dose range 0.5–25 kGy. Thus, it can be used for estimation of the dose magnitude and in discrimination of irradiated SA and/or SA containing compounds from unirradiated ones. To examine the utility of the derived equations, back-calculated doses were obtained by entering the measured peak heights in the equations described above. It was concluded that 5 and 15 kGy applied doses could be estimated with an accuracy of 5% and 6%, respectively, when the polynomial function obtained after fitting the experimental intensity data relevant to I_2 was used. However, influences of water and oxygen contents and storage time on signal intensity must be elaborated in detail to ascertain these results.

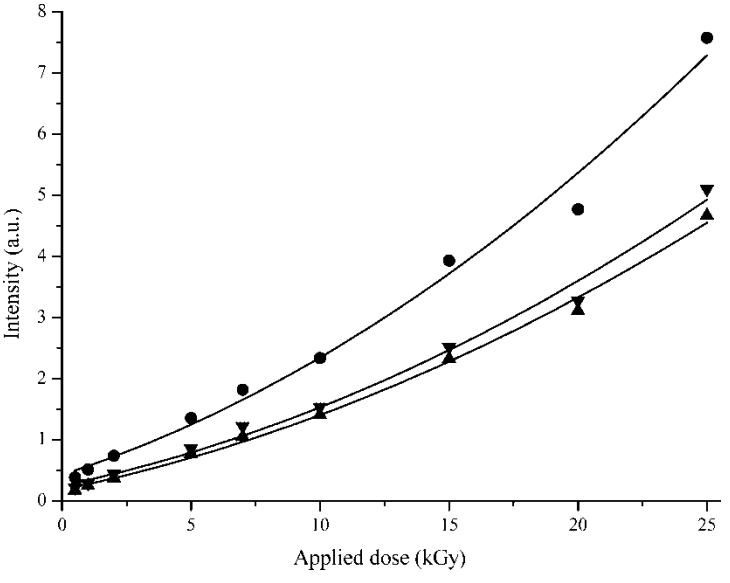

Figure 6. Variations of the measured intensities with applied radiation dose. Experimental, •(I_2); ▲(I_4); ▼(I_5); calculated using polynomial function, solid lines.

Table 1. Parameters and correlation coefficients calculated for denoted signal intensities by fitting experimental dose–response data to three different mathematical functions.

		Resonance peaks		
Function	Parameter	I_2	I_4	I_5
$I = a + bD$	a	0.0395	−0.0635	−0.0281
	b	0.2698	0.1717	0.1838
	r^2	0.9702	0.9777	0.9719
$I = k + lD + mD^2$	k	0.4294	0.1840	0.2498
	l	0.1364	0.0871	0.0887
	m	0.0055	0.0035	0.0040
	r^2	0.9884	0.9958	0.9918
$I = n(1 - e^{-pD})$	n	289.1305	209.1662	215.1088
	p	0.0010	0.0008	0.0009
	r^2	0.9693	0.9760	0.9709

3.5 *Annealing studies at high temperature*

Irreversible decreases in ESR intensities at high temperatures would be expected to originate from the decay of radical species contributing to the formation of the experimental spectrum. Besides, the decay rates of these units should depend on the sample temperature. Thus, variations of the line intensities at high temperatures were studied to obtain information about the kinetic features of the radicals produced in irradiated SA. Measurements were taken on experimental spectra recorded at annealing temperature without cooling the sample to room temperature as is often done to avoid any drawback originating from sample positioning in the microwave cavity. Data derived at four different temperatures (370, 380, 390, and 400 K) for the I_2 intensity of a sample irradiated at 10 kGy are given in figure 7 as an example of these variations. Similar variations were obtained for other line intensities, but to save space they are not presented in the present work. Decreases in the intensities 380 K are faster. A total of 19% and 73% intensity decreases were calculated to occur at the end of 65 min annealing treatment at annealing temperatures of 380 and 400 K, respectively. The experimental decay data obtained for each line intensity were fitted to a function consisting of the sum of two exponentially decaying functions of different relative weights assuming that the involved radical species undergo first-order kinetics and the decay constants of the latter were calculated at four different temperatures. The results obtained for the I_2 intensities are given in table 2. Calculated decay constants given in this table were used to derive theoretical variation curves of the line intensities with annealing time at each annealing temperature. The results relevant to the I_2 intensity are presented in figure 7 with their experimental counterpart for comparison. As is seen, both the experimental and theoretical results are in good agreement for the I_2 intensity, and that also was the case for other studied line intensities. Activation energies of the involved species were also calculated from $\ln(k) - T^{-1}$ graphs and the following values were obtained for species A and B: $E_A = 165.84$ kJ/mol and $E_B = 107.38$ kJ/mol, respectively.

3.6 *Simulation calculations and proposed tentative radical species*

AA and SA crystallize in $P2_1$ and $P2_12_12_1$ space group symmetries, respectively, and both of them contain four molecules in their unit cells [17, 18]. The four molecules in the unit cell of AA are related in pairs by pseudo screw axes. While the lactone group is moderately corrugated in AA, the whole ring system of SA, except for C(3) and O(3) atoms, has been

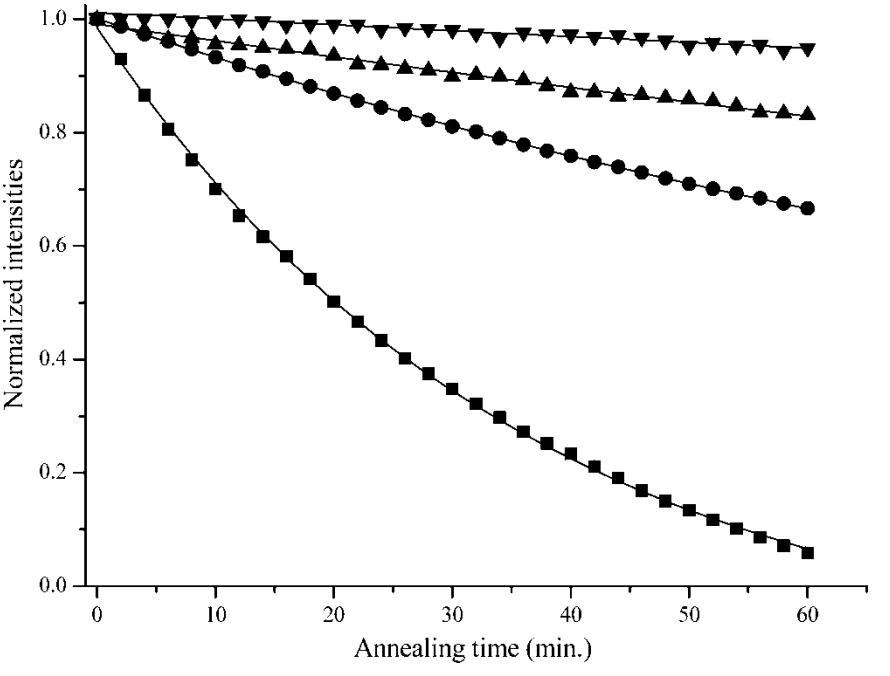

Figure 7. Variations of the I_2 intensity for a sample irradiated at dose of 10 kGy with annealing temperature and annealing time. Experimental, ▼(370 K), ▲(380 K), •(390 K), ■(400 K); theoretical (calculated using parameters given in table 2), solid lines.

Table 2. Decay constants and relative contribution weights calculated for responsible radical species at four different annealing temperatures.

Annealing temperature (K)	Species	Contribution weights of the species to I_2 intensity %	Decay constants (min^{-1})
370	A	0.2001	0.00109
	B	0.8024	0.00110
380	A	0.1888	0.00526
	B	0.7736	0.00241
390	A	0.1888	0.01636
	B	0.7569	0.00509
400	A	0.1788	0.06688
	B	0.7342	0.01587

shown to be maintained in aqueous solution after circular dichroism and nuclear magnetic resonance measurements carried out by Kresheck (1968, private communication).

According to Van Euler and Eister [19] and Hvoslef [18], the ascorbate anion may be described as a mesomer among slightly different molecular structures. In accordance with this finding, as in the case of AA [10, 13], the following radical species of different g parameters (but, due to conformational changes exhibited by the ascorbate anion, not presenting significant hyperfine interactions) were assumed to be responsible for relatively narrow (1.5 mT) ESR spectrum of gamma irradiated SA. Thus, the spectrum simulation calculations based on the presence of two different species where performed to get g parameters of the contributing radical species. Signal intensity data gathered from room temperature spectra were used as input in these calculations.

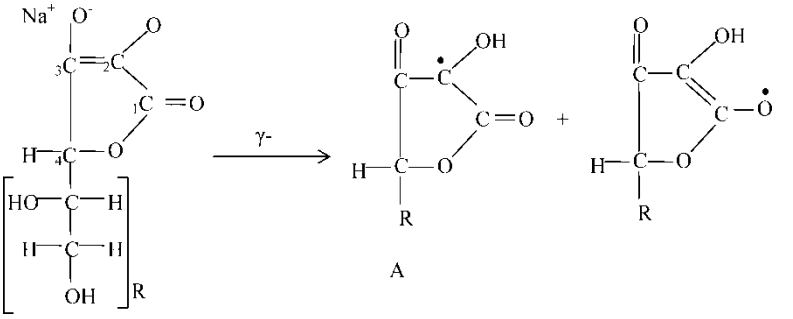

SCHEME 1

Table 3. Spectroscopic parameters calculated for proposed tentative radical species.

Species	Concentration (%)	ΔH_{pp} (mT)	g-values		
			g_{xx}	g_{yy}	g_{zz}
A	0.567	0.555	2.0048	2.0062	2.0059
B	0.433	0.336	2.0110	2.0000	2.0028

The results are presented in table 3. The theoretical spectrum of each contributing specie and their sum were also calculated using spectroscopic parameters derived from simulation calculations (table 3). The results are presented in figure 8. It is seen that the theoretical and experimental sum spectra are in good agreement and that a model based on the presence of two different radical species of different kinetic and spectroscopic features describes very well

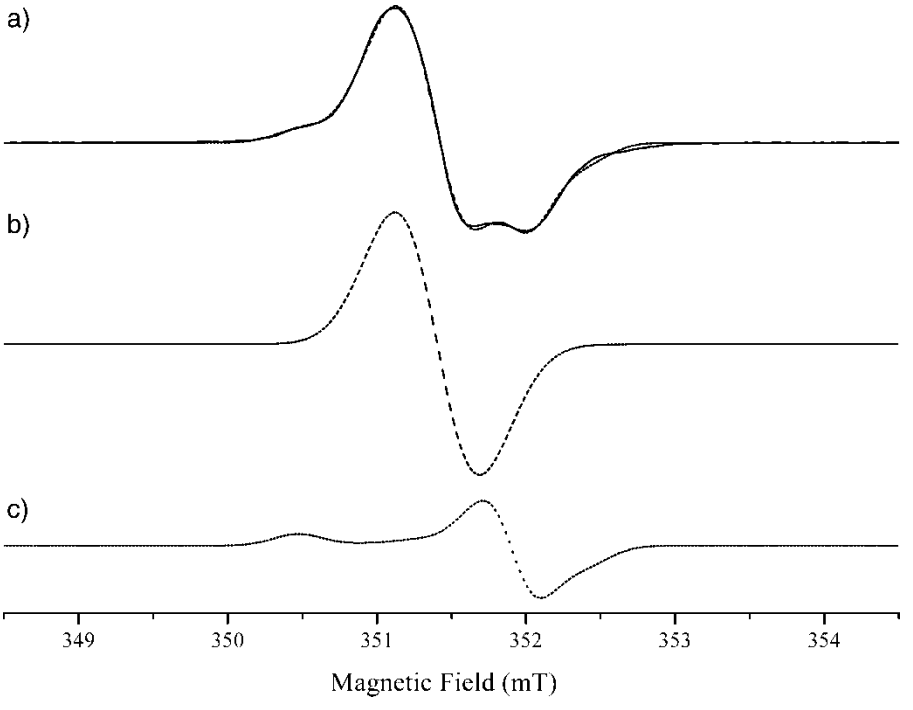

Figure 8. Experimental (solid line) and theoretical (dashed line) ESR spectra calculated using parameter values given in table 3. (a) sum spectra; (b) species A; (c) species B.

the observed experimental spectrum. From table 3 and figure 8, it is seen that the proton of the hydroxyl group bond directly to the C(2) carbon atom contributes to line broadening rather than creating resolved detectable hyperfine splitting in the ESR spectra of both species. But, the line broadening is more pronounced in the case of species A due to the shorter distance between unpaired electrons of the latter species and the hydroxyl proton.

4. Conclusion

The ESR spectra of gamma irradiated SA is very different from that obtained for AA although both compounds contain four molecules in their unit cells. This is due to the fact that these compounds crystallize in different crystal symmetries. The ESR spectrum of SA presented in this work is also different from the spectrum reported by Basly *et al.* [11] for the same compound. Homogeneously, broadened resonance line characteristics of the observed dominant ESR intensities were considered as an indication of the presence of species not having very high g factor anisotropy. From the long-term (90 days) kinetic studies at room temperature, it was concluded that the involved species were fairly stable at room temperature and that irradiated and unirradiated SA could be very easily discriminated even at the end of a 90-day storage period. A polynomial function of the applied dose (D) was found describing best the dose–response data in the range of 0.5–25 kGy with accuracy better than 6%. Based on these findings, it was concluded that SA can be used in the estimation of the dose range in accidental dosimetry and that irradiated SA can be easily distinguished from unirradiated one, which is very important for trade control. A model based on the presence of two radical species exhibiting different kinetic and spectroscopic features were calculated to describe fairly well the results of annealing studies performed at high temperatures and the signal intensity data of the experimental ESR spectrum.

Acknowledgements

This work was supported by the Scientific Research Foundation of Hacettepe University.

References

[1] G.W. Gould, New Methods of Food Preservation. (Blackie Academic and Professional, Glasgow, 1995).
[2] WHO, Report of a Joint FAO/WHO/IAEA Expert Committee. Technical Report Series No. 659, World Health Organization Geneva, Switzerland (1981).
[3] G.A. Schreber, N. Helle and K.W. Bögl, Int. J. Radiat. Biol. **63**(1) 105–130 (1993).
[4] L. Douifi, J. Raffi, P. Stocker *et al.*, Speactrochim. Acta A **54**(14) 2403–2413 (1998).
[5] WHO, Report of a Joint FAO/WHO/IAEA Expert Committee. Technical Report Series No. 890, World Health Organization Genova, Switzerland (1999).
[6] E.M. Stewart, Detection Methods for Irradiated Foods (John Wiley and Sons, New York, 2001), pp. 347–386.
[7] M.F. Desrosiers, Appl. Radiat. Isot. **47**(11–12) 1621–1628 (1996).
[8] M.F. Desrosiers, S.L. Cooper, J.M. Puhl *et al.*, Radiat. Phys. Chem. **71** 365–370 (2004).
[9] L. Sun-Young, Int. J. Food Saf. **3** 32–35 (2004).
[10] M. Korkmaz and M. Polat, Improving the safety of fresh fruit and vegetables (Woodhead Publishing Limited, Cambridge, 2005), pp. 387–428.
[11] J.P. Basly, I. Longy and M. Bernard, Anal. Chim. Acta **372** 373–378 (1998).
[12] M. Polat and M. Korkmaz, Anal. Chim. Acta **535** 331–337 (2005).
[13] H.N. Rexroad and W. Gordy, Proc. Natl. Acad. Sci. **45** 256–269 (1959).
[14] M.F. Desrosiers, Appl. Radiat. Isot. **42** 617–619 (1991).
[15] N.J.F. Dodd, J.S. Lea and A.J. Swallow, Nature **334** 387–388 (1988).
[16] M.F. Desrosiers, G.L. Wilson, C.R. Hunter *et al.*, Appl. Radiat. Isot. **42** 613–616 (1991).
[17] J. Hvoslef, Acta Cryst. B **24** 23–35 (1968).
[18] J. Hvoslef, Acta Cryst. B **25** 2214–2223 (1969).
[19] H. von Euler and B. Eistert, Chemie and Biochemie der Reduktone und Reduktonate (Stuttgart, 1957), p. 24.